energies

MDPI

Article

Ride-Through Control Method for the Continuous Commutation Failures of HVDC Systems Based on DC Emergency Power Control

Chao Xiao [1,*], Wei Han [1], Jinxin Ouyang [2], Xiaofu Xiong [2] and Wei Wang [2]

1 State Grid Henan Electric Power Research Institute, Zhengzhou 450052, China; hnlhhw@126.com
2 State Key Laboratory of Power Transmission Equipment & System Security and New Technology, Chongqing University, Chongqing 400044, China; exphujian@foxmail.com (J.O.); xc0212@foxmail.com (X.X.); cquwangwei@cqu.edu.cn (W.W.)
* Correspondence: sngeet@163.com

Received: 13 August 2019; Accepted: 19 September 2019; Published: 2 November 2019

Abstract: Continuous commutation failures (CFs) are serious malfunctions in line-commutated converter high-voltage direct current (HVDC) systems that cause the continuous and rapid sag of transmitted power and may threaten the stability of AC systems. The conventional emergency control strategies of AC systems exhibit difficulty in responding quickly and accurately. After suffering from continuous CFs, the forced blocking of direct current (DC) converter to prevent AC system instability might also cause other adverse effects. This study proposes a ride-through control method to improve the endurance capability of AC systems against continuous CFs. An active power output model of inverter station under continuous CFs is built, while considering the process and mechanism of CFs. The impact of continuous DC power sag on the stability of sending-end system is analyzed through a four-area AC/DC equivalent model. A rolling calculation model for the power angle and acceleration area variations of the sending-end system during continuous CFs is established on the basis of model predictive control theory. A calculation method for the emergency power control reference is obtained by using the aforementioned models. Lastly, a ride-through control method for continuous CFs is developed by utilizing the emergency control of adjacent HVDC link. Simulation results show that the proposed control method can improve the endurance capability of an AC system to continuous CFs and reduce blocking risk in an HVDC link.

Keywords: High voltage direct current (HVDC); continuous commutation failures; DC blocking; emergency power support; stability

1. Introduction

With the rapid development of large-capacity high-voltage direct current (HVDC) transmission technology and the accelerating construction of HVDC projects, hybrid AC/DC power grids are rapidly developing [1,2]. For a large-scale asynchronous grid interconnected by DC systems, the dynamic response of a DC system exerts an increasingly significant impact on an AC grid due to the increased level of DC power transmission capacity. Commutation failure (CF) is a frequent dynamic event in an HVDC system that is generally caused by a disturbance in an AC grid. During CF, the transmitted power of a DC system is considerably reduced, which will affect the stability margin of an AC grid and seriously threaten the safe operation of a power system [3–5].

In recent years, the impact of HVDC CF on the safety and stability of an AC power grid has elicited increasing attention [6–12]. The influence mechanism of CF on the stability of a sending-end AC grid was investigated in [6]. To overcome the instability problem caused by CF, control measures,

such as setting a delay time when reclosing a device or implementing generator tripping from the sending-end grid, were proposed in [7,8] to improve the stability of an AC grid. In [9], a scheme for solving the problem of simultaneous and multiple HVDC CFs was proposed, and field tests verified that the system can satisfy power grid stability control requirements. The recovery time of generators after tripping was generally tens of minutes; however, the duration of a single CF only lasted 160–200 ms [10]. When the commutation process of a DC system returns to normal, the low power recovery rate will result in continuous power imbalance in an AC grid. In consideration of the fast power control capability of a DC system [11], a DC power compensation modulation method that is implemented after CF recovery was proposed in [12]; this method can reduce tripped generator capacity in a sending-end system. The aforementioned studies focused on control methods that can address the impact of a single CF.

If a receiving-end system is weak or if grid fault lasts for a long time, then continuous CFs may occur in an HVDC system. A power sag caused by continuous CFs has a short duration and a large amplitude. Thus, quantifying power variations during continuous CFs is difficult, and emergency control strategies for continuous CFs lack an effective quantitative control method. To avoid AC system instability during continuous CFs, converter stations are forcibly blocked once CF frequency reaches a certain number of times. For example, in practical HVDC systems in East China, HVDC converter stations are blocked once continuous CFs are detected thrice [13]. However, if a DC system can recover after several continuous CFs, then its forced blocking may lead to large-scale generator tripping, load shedding, and long-term recovery. If the stability of an AC system can be guaranteed by an emergency control strategy during continuous CFs, then the risk of DC blocking caused by continuous CFs can be reduced. Once the commutation process returns to normal, a system can recover quickly and ride through continuous CFs.

In a multi-paralleled DC system scenario, the risk of CF varies with different locations and a DC system without CF provides an important means of emergency power control for an AC system. Accordingly, a ride-through control method for continuous CFs in an HVDC system based on model predictive control (MPC) theory is presented in the current study. First, an active power output model of a DC inverter under continuous CFs is established by analyzing the CF process. Then, the impact of a transmitted power sag on the stability of a sending-end system during continuous CFs is determined. Subsequently, a rolling calculation model of the equivalent rotor angle and acceleration area variation of a sending-end system during DC continuous CFs is established in accordance with MPC theory. The calculation method for the emergency power control reference is then obtained by considering the aforementioned models. Finally, a ride-through control method for continuous CFs is developed through the emergency control of adjacent HVDC, case studies are performed in MATLAB/SIMULINK to verify the effectiveness of the proposed control method.

2. Analysis of Power Characteristics during DC Continuous CFs

Commutation failure is a frequent dynamic event in the LCC-HVDC system. CF is considered to occur when a thyristor valve that is supposed to be turned off, continues to conduct current without transferring it to the next valve in the firing sequence [14]. CF occurs in a rectifier only if the firing circuit fails.

For a six-pulse inverter, valves 1 to 6 are turned on in sequence at a normal interval of 60°. When CF occurs, CF from valves 1 to 3 is used as an example. If the voltage drop occurs before the triggering moment of the valve 3, the valve 1 is not extinguished normally, current in valve 3 will decrease to zero and the valve will extinguish. When valve 4 fires next, because valve 1 is still conducting, a short circuit is placed across the DC side of the bridge. The zero DC voltage keeps the voltage across valve 5 negative so that valve 5 cannot conduct. Valve 4 is extinguished and valve 6 is ignited in the normal fashion [15]. For the period when valves 1 and 4 are both conducting, the inverter DC voltage is zero and the corresponding electrical angle is $120° + \mu$, where, μ is the overlap angle. The reduction of the extinction angle and the increase in DC current during grid fault will trigger the

extinction angle controller and the voltage-dependent current order limiter (VDCOL). If CF is within the range of DC regulation, then the CF process returns to normal; otherwise, continuous CFs occur.

In accordance with the DC converter station control equation, the DC voltage and transmitted active power at the inverter side can be expressed as follows:

$$U_d = N_c\left(1.35U_B\cos\gamma - \frac{3}{\pi}X_cI_d\right) \tag{1}$$

$$P_d = N_c\left(1.35U_B\cos\gamma - \frac{3}{\pi}X_cI_d\right)I_d \tag{2}$$

where N_c is the number of six-pulse thyristor bridge converter at inverter side, U_B is the RMS voltage of AC system on the inverter side, I_d is the DC current, γ is the extinction angle of inverter, X_c is commutating reactance, U_d is the DC voltage at inverter side, P_d is the transmitted active power by inverter station.

During AC voltage sag, the DC current reference value of line-commutated converter HVDC is determined by the VDCOL control characteristic:

$$I'_d = \begin{cases} I_{dl} & , U_d \le U_{dl} \\ \frac{I_{dh}-I_{dl}}{U_{dh}-U_{dl}}U_d + \frac{U_{dh}I_{dl}-U_{dl}I_{dh}}{U_{dh}-U_{dl}}, & U_{dl} < U_d \le U_{dh} \\ I_{dh} & , U_{dh} \le U_d < U_{rated} \end{cases} \tag{3}$$

where I_{dl} and I_{dh} are the minimum and maximum DC current reference value, respectively; U_{dl} and U_{dh} are the DC voltage thresholds value, U_{rated} is the rated DC voltage.

Continuous CFs typically occur during the recovery process, and the maximum transmitted power during CF recovery is determined by the magnitude of AC fault voltage reduction and DC current. In accordance with (1), when the extinction angle $\gamma = 0$, the maximum transmitted active power can be obtained by

$$P_{d1} = N_c\left(1.35U'_B - \frac{3}{\pi}X_cI'_d\right)I'_d \tag{4}$$

where U'_B is RMS voltage at the AC side of the inverter station at the initial time of grid fault, P_{d1} is maximum transmitted active power during grid fault.

Given that the period of the CF recovery process is short and the power variation rate is high, the power recovery process can be approximated as linear. Accordingly, the variation in transmitted power by a DC inverter station under continuous CFs is shown in Figure 1, where, P_{d0} is the transmitted active power by inverter station under steady state conditions. The transmitted power sag duration ΔT caused by CF is affected by the control parameters of the rectifier and inverter station, which are generally 160–200 ms [16]. The duration of the zero transmitted power ΔT_1 is generally 10 ms based on the period when DC voltage is zero during CF. When continuous CFs occur, the amplitude of the AC voltage reduction will be greater, the transmitted power recovery peak value P_{d1} will be smaller, and CF recovery time will be shorter. When the commutation process returns to normal, DC transmitted power will be restored to the steady-state value P_{d0}.

During continuous CFs, the transmitted active power of a DC inverter can be expressed as:

$$P_d = \begin{cases} P_{d0} & t \in [0, t_1) \\ 0 & , t \in [t_1, t_1 + j\Delta T_1 + (j-1)\Delta T_2) \\ \frac{P_{d1}(t-t_1-j\Delta T_1-(j-1)\Delta T_2)}{\Delta T_2} & , t \in [t_1 + j\Delta T_1 + (j-1)\Delta T_2, t_1 + j\Delta T_1 + j\Delta T_2)(j < N) \\ \frac{P_{d0}(t-t_1-j\Delta T_1-(j-1)\Delta T_2)}{\Delta T_2}, & t \in [t_1 + j\Delta T_1 + (j-1)\Delta T_2, t_1 + j\Delta T_1 + j\Delta T_2)(j = N) \\ P_{d0} & , t \in [t_1 + N\Delta T_1 + N\Delta T_2, \infty) \end{cases} \tag{5}$$

where t_1 is the time of first CF occurs, and j is the frequency of continuous CFs, $j = 1, 2, 3, \ldots, N$.

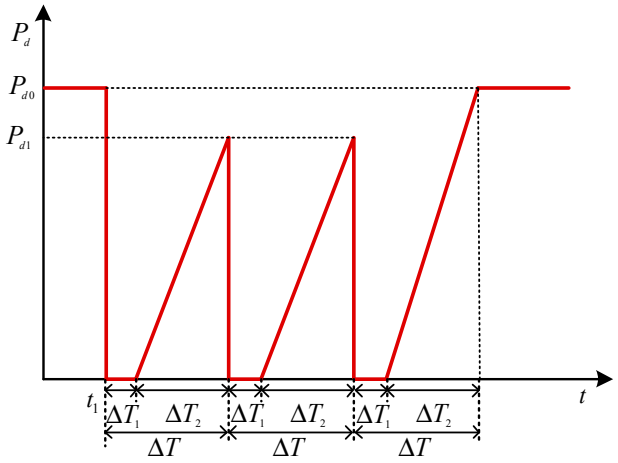

Figure 1. Transmitted power of DC inverter under continuous commutation failures (CFs).

3. Effect of Continuous CFs on Sending-end Grid

Figure 2 shows a schematic of a four-area AC/DC interconnected equivalent model. Under steady-state operation, the sending-end and receiving-end grids are connected by two DC links. x_1 and x_2 are the equivalent reactance of generators G1 and G2, respectively; x_{12} is the tie line reactance between bus B1 and bus B2; $E_{s1} \angle \delta_{s1}$ and $E_{s2} \angle \delta_{s2}$ are the internal potential and rotor angle of equivalent generators G1 and G2, respectively; U_1 and U_2 are the voltage amplitude at bus B1 and B2, respectively; θ_1 and θ_2 are the phase angle at bus B1 and B2, respectively; P_{G1} and P_{G2} are the output mechanical power of the equivalent generators, respectively; P_{L1} and P_{L2} are the load power represented by L1 and L2, respectively; P_{12} is the transmitted power from bus B_1 to bus B_2; P_{DC1} and P_{DC2} are the transmitted power by DC_1 and DC_2 inverter station, respectively.

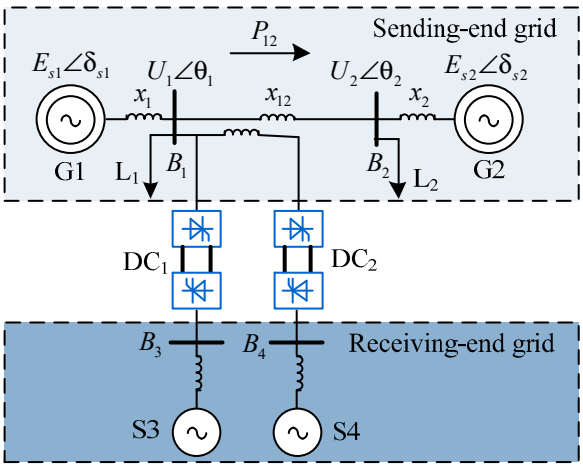

Figure 2. Equivalent model of AC/DC interconnected system.

The rotor motion equation of the equivalent generators G1 and G2 can be expressed by [17]

$$\begin{cases} \frac{T_{J1}}{\omega_0}\frac{d^2\delta_{s1}}{dt^2} = P_{G1} - P_{DC} - P_{L1} - \frac{U_1 U_2 \sin(\theta_1-\theta_2)}{x_{12}} \\ \frac{T_{J2}}{\omega_0}\frac{d^2\delta_{s2}}{dt^2} = P_{G2} - P_{L2} + \frac{U_1 U_2 \sin(\theta_1-\theta_2)}{x_{12}} \end{cases} \quad (6)$$

where T_{J1} and T_{J2} are the inertia time constants of equivalent generator, respectively. ω_0 is the rated angular velocity, P_{DC} is the sum of the active power transmitted by all DC links.

Assume that the interconnection between areas 1 and 2 is weak, then the reactance of tie line x_{12} is considerably larger than equivalent generator reactance. Then, $\theta_1 \approx \delta_{s1}$ and $\theta_2 \approx \delta_{s2}$ can be approximated.

By subtracting the two formulas in (6), the equivalent single machine rotor motion equation can be given by

$$\frac{d\delta^2}{dt^2} = P_m - P_{e\max} \sin\delta \tag{7}$$

where δ is the rotor angle deviations between G1 and G2, $\delta = \delta_{s1} - \delta_{s2}$.

The equivalent mechanical power P_m can be obtained as

$$P_m = \left(\frac{P_{G1}}{M_1} - \frac{P_{G2}}{M_2}\right) - \left(\frac{P_{L1}}{M_1} - \frac{P_{L2}}{M_2}\right) - \frac{P_{DC}}{M_1} \tag{8}$$

The peak value of equivalent electromagnetic power $P_{e\max}$ can be obtained as

$$P_{e\max} = \left(\frac{1}{M_1} + \frac{1}{M_2}\right)\frac{U_1 U_2}{x_{12}} \tag{9}$$

where $M_1 = T_{J1}/\omega_0$, $M_2 = T_{J2}/\omega_0$.

Assume that j times continuous CFs are caused by a short circuit fault at bus B3. Then, the voltage magnitude at bus B4 is less affected and DC_2 can continue operating in normal state. In accordance with (7–9), the power characteristic curve during the continuous CFs of DC_1 is illustrated in Figure 3. Where, A_a and A_d are acceleration area and deceleration area caused by continuous CFs.

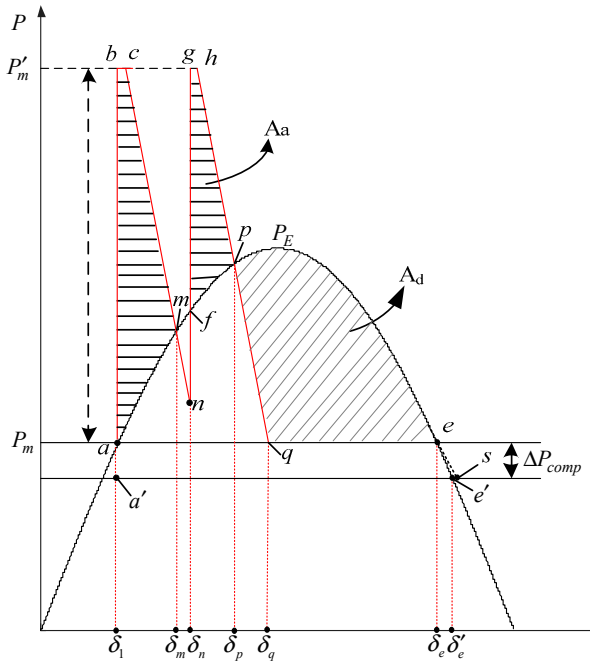

Figure 3. Power characteristic curve of sending-end grid under continuous CFs.

Before CF occurs, the steady-state operating point is a and its corresponding rotor angle is δ_1. As shown in (7–9), continuous CFs cause a continuous sag of the power transmitted by DC_1, thereby increasing the equivalent mechanical power P_m to P'_m. During the period when the equivalent mechanical power is greater than the electromagnetic power, the rotor accelerates and the rotor angle δ is gradually increased. Consequently, the operating point moves along the power curve from point a to point m, and the corresponding acceleration area is A_{abcm}. During CF recovery, the equivalent electromagnetic power becomes gradually higher than the equivalent mechanical power, and the

rotor starts to decelerate. However, the rotor angle δ will continue increasing to point f, and the corresponding deceleration area is A_{mnf}.

Similarly, the rotor angle δ in the j-th CF process will gradually increase during the period when the equivalent mechanical power P_m is higher than the equivalent electromagnetic power due to the transmitted power sag. The operating point f moves along the power curve to point p, and the acceleration area is A_{fghp}. After the time of point p, the equivalent mechanical power is less than the electromagnetic power. The rotor speed decelerates, but the rotor angle continues to increase gradually. The operating point continues to move along the electromagnetic power curve from point p until the deceleration area becomes equal to the acceleration area. Thereafter, the rotor angle reaches its maximum value and starts to decrease gradually.

If the deceleration area A_{pqe} remains smaller than the cumulative acceleration area when the operating point moves to point e, then the sending-end system will lose stability. The requirement for maintaining the stability of the sending-end grid during continuous CFs is that the cumulative acceleration area should be smaller than the deceleration area; that is,

$$A_{abcm} + A_{fghp} < A_{pqe} \tag{10}$$

4. Emergency Power Support Control for System Transient Stability

4.1. Control Principle

Given the constant variation in equivalent mechanical power during continuous CFs, an accurate calculation of the rotor angle and the acceleration area is difficult. Therefore, the equivalent mechanical power and electromagnetic power curve are piecewise linearized following a certain step size, and the power angle and acceleration area variations of the sending-end system can be obtained point-by-point. When CF is detected, the emergency power control reference is obtained on the basis of the relative magnitudes of the acceleration area and deceleration area. According to the model predictive control theory [18], the feedback correction calculation of the rotor angle and acceleration area variations of the sending-end system considering the emergency power control is performed. Subsequently, a closed loop rolling control process is achieved. When the next CF is detected, the maximum rotor angle variation of the sending-end system obtained in the first CF process is set as the initial rotor angle for the next CF, and the deceleration area is corrected. The amount of emergency power control can be calculated to ensure the stability of the sending-end system. Therefore, the DC system that occurs during continuous CFs should not be forced blocked immediately, and DC blocking risk due to continuous CFs is reduced. The basic principle of the proposed emergency power control is illustrated in Figure 4.

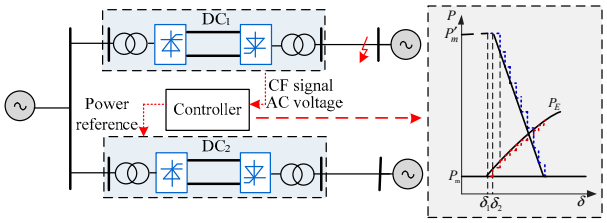

Figure 4. DC emergency power control schematic diagram.

4.2. Calculation of Emergency Power Control Reference

The emergency power control reference can be obtained as follows.

Step 1: Following (6–8), the rotor angle δ_1 that corresponds to the steady-state operating point a and the rotor angle δ_e that corresponds to the stability critical point e can be obtained. When the first CF signal is detected, the number of continuous CFs j is set as 1. The variation process of the equivalent mechanical power and the electromagnetic power caused by one CF is divided into n cycles for piecewise

linearization in steps of Δt, where Δt is set as 10 ms. Thus, the sampled horizon is $[t_1, t_2, t_3, \cdots, t_n]$, where t_1 is the time when the first CF is detected, and $n = \Delta T/\Delta t$, $t_n = t_1 + (n-1)\Delta t$. P'_{mi} and $P_{e\max} \sin \delta_i$ are the equivalent mechanical power and the electromagnetic power that correspond to sampling point i, respectively.

Let i = 1. By integrating the formula (7) for rotor motion, the analytical expression of δ_{i+1} can be given by

$$\delta_{i+1} = \frac{1}{2}(P'_{mi} - P_{e\max} \sin \delta_i)\Delta t^2 + \delta_i \tag{11}$$

In accordance with (11), the sequence of the equivalent rotor angle of the sending-end system that corresponds to each sample point in the process of the first CF can be obtained as $[\delta_1, \delta_2, \cdots, \delta_m, \cdots, \delta_n]$, where δ_m represents the maximum rotor angle value during the acceleration process.

Step 2: The estimated acceleration area for the j-th CF can be given by

$$A_{a\_j} = \sum_{i=1}^{m-1} \int_{\delta_i}^{\delta_{i+1}} (P'_{mi} - P_{e\max} \sin \delta) d\delta \tag{12}$$

The deceleration area A_{d} in the interval (δ_n, δ_e) can be obtained as

$$A_d = \int_{\delta_n}^{\delta_e} (P_{e\max} \sin \delta - P_m) d\delta \tag{13}$$

Step 3: In the calculation of the deceleration area in equation (13), the deceleration area A_{mnf} in each recovery process of CF is neglected. Therefore, a certain stability margin can be guaranteed with the emergency control reference obtained by directly comparing the acceleration area with deceleration area. If $A_{a\_j} \le A_d$, then the emergency power control reference is set as zero, $P_{em\_j} = 0$. If $A_{a\_j} > A_d$, then the emergency power control reference P_{em_j} is obtained by comparing the relative magnitudes of A_{a_j} and A_d.

As shown in Figure 3, the unstable points before and after the emergency power control is implemented are assumed to be e and e', respectively. The electromagnetic power variation in this interval can be approximated by a straight-line es. The intersection of the electromagnetic power and the mechanical power is point e, and the tangential slope of the electromagnetic power curve at point e is k; thus,

$$k = \frac{P_{em\_j}}{\delta_e - \delta_{e'}} \tag{14}$$

To achieve the acceleration area, the deceleration area that should be increased under emergency power control is

$$\Delta A_{d\_j} = A_{a\_j} - A_d \approx \frac{1}{2}(\delta_e + \delta_{e'} - 2\delta_1) P_{em\_j} \tag{15}$$

When (14) and (15) are combined, the rotor angle value $\delta_{e'}$ at point e' and the emergency power control reference P_{em_j} can be obtained. P_{em_j} can be calculated as

$$P_{em\_j} = \sqrt{-2k\left(A_{a\_j} - A_d\right) + k^2(\delta_e - \delta_1)^2} + k(\delta_e - \delta_1) \tag{16}$$

Step 4: If the maximum emergency power support capacity $\Delta P_{\mathrm{DC\_max}}$ of DC_2 is equal to or higher than P_{em_j}, then P_{em_j} is selected as the DC emergency control reference. Otherwise, if $\Delta P_{\mathrm{DC\_max}}$ is less than P_{em_j}, then the maximum DC emergency control capacity is applied. The selective tripping of generating units should also be used to satisfy the stability control requirement, and the minimum generator tripping capacity is $\Delta P_{comp} = P_{em\_j} - \Delta P_{\mathrm{DC\_max}}$.

Step 5: In accordance with (11) and considering the obtained emergency power control reference P_{em_j}, the rotor angle variation sequence of the j-th CF period is corrected as $[\delta_1, \delta'_2, \cdots, \delta'_m, \cdots, \delta'_n]$.

Considering the emergency power control, the acceleration area A'_{a_j} is given as

$$A'_{a\_j} = \sum_{i=1}^{m-1} \int_{\delta'_i}^{\delta'_{i+1}} \left(P'_{mi} - P_{em\_j} - P_{e\max} \sin\delta\right) d\delta \tag{17}$$

Step 6: If no continuous CF is detected, then the emergency power control will exit; otherwise, if continuous CFs are detected, then let $j = j + 1$ and set the maximum rotor angle variation calculated in the $(j-1)$-th CF process as the initial rotor angle of j-th CF. Equation (18) indicates that the equivalent rotor angle variation of the sending-end system that corresponds to each sampling point during the j-th CF can be calculated as $[\delta_1, \delta_2, \cdots, \delta_m, \cdots, \delta_n]$.

$$\delta_{i+1} = \frac{1}{2}\left(P'_{mi} - P_{em\_j-1} - P_{e\max} \sin\delta_i\right)\Delta t^2 + \delta_i \tag{18}$$

Therefore, the acceleration area for the j-th CF can be given by

$$A_{a\_j} = \sum_{i=1}^{m-1} \int_{\delta_i}^{\delta_{i+1}} \left(P'_{mi} - P_{em\_j-1} - P_{e\max} \sin\delta_i\right) d\delta \tag{19}$$

The accumulated acceleration area produced by continuous CFs is

$$A_a = A_{a\_j} + \sum_{j=1}^{j-1} A'_{a\_j} \tag{20}$$

The deceleration area A_{d_j} in the interval $(\delta_n, \delta_{e'})$ can be obtained as:

$$A_{d\_j} = \int_{\delta_n}^{\delta_{e'}} \left(P_{e\max} \sin\delta - P_m - P_{em\_j-1}\right) d\delta \tag{21}$$

Step 7: By combining the acceleration and deceleration areas after the j-th CF, the additional emergency power control reference P_{em_j} can be calculated using (16). Thus, the emergency power control reference when the j-th CF occurs can be obtained by

$$P_{em} = P_{em\_j} + \sum_{j=1}^{j-1} P_{em\_j} \tag{22}$$

In accordance with the obtained emergency power control reference, return to Step 5 for the correct calculation of the rotor angle variation and the acceleration area.

If no continuous CFs are detected, then the emergency power control will exit; otherwise, Steps (6–7) will be repeatedly executed. If $\delta_n \geq \delta_{e'}$, then the stability margin of the sending-end system is low, the DC converter should be actively blocked, and the stability control strategy should be adopted. On the basis of the aforementioned emergency power control strategy during continuous CFs, the stability of the first swing of the sending-end grid can be improved to the greatest extent, and the amount of generator tripping can be reduced. Furthermore, the risk of converter blocking due to the first swing angle instability of the sending-end grid during continuous CFs can be reduced. If the continuous CF process can return to normal, then the system can immediately recover to normal operation.

When continuous CFs occurs in one of DC links, the flowchart of DC emergency power control is shown in Figure 5. During continuous CFs, the emergency power support control of an adjacent non-CF DC system can reduce the equivalent mechanical power variation and improve the first swing transient stability of the sending-end system; however, the HVDC emergency control should exit on

time to avoid the adverse effects on the reverse swing stability [19,20]. Considering that the first swing instability mode after the disturbance generally occurs approximately 1.5 s after the fault [21], the exit time of the DC emergency power control is set as 1.5 s after the fault. In addition, considering the time delay of CF detection and AC voltage acquisition, the implementation time of the proposed control method will slightly lag behind the actual occurrence time of CF. However, the control method is a continuous dynamic adjustment process. The time delay due to signal acquisition and transmission does not affect the regulation trend of the emergency control.

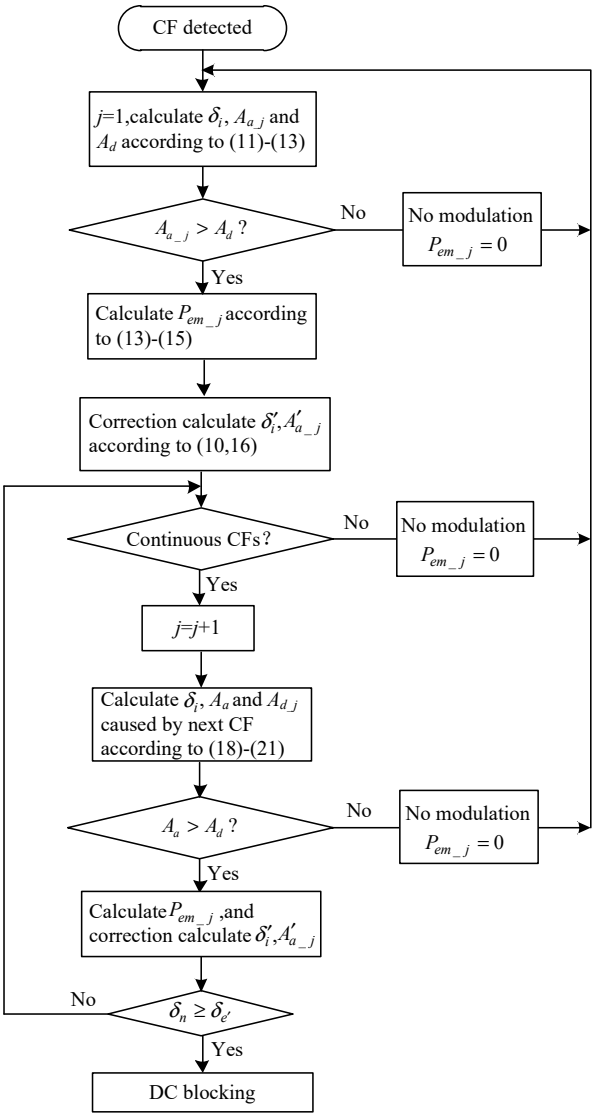

Figure 5. Flow chart of DC emergency power control.

5. Simulation Analysis

To validate the performance of the proposed control method, case studies on the AC/DC interconnection system (Figure 2) are conducted using MATLAB/Simulink. The system parameters are as follows. The system base capacity is 100 MW, the rated frequency is 50 Hz, and the RMS voltage of AC grid is 230 kV. Four synchronous generators are found in G1. Two of the generators have an output power of 10.0 p.u., capacity of the other two generators are 2.0 p.u. and 4.0 p.u., respectively. G2 contains a synchronous generator with an output power of 10.0 p.u. The inertia time constants of each generator in sending-end grids are 3.2 s. The receiving-end grids S3 and S4 are modeled with the voltage sources and series impedance for the sake of simplicity, and the short circuit ratio

(SCR) of receiving-end grid is 2.5, respectively. Load capacity of L1 and L2 are 2.2 p.u. and 13.8 p.u., respectively. Each DC link adopts 12-pulse converter and DC rated transmitted power is 10.0 p.u., respectively. The rectifier side adopts the constant current control, while the inverter side adopts the constant extinction angle control and constant current control. The reactance x_{12} of tie-line between bus B1 and B2 is 87 Ω. The parameters of VDCOL are I_{dl} and I_{dh} are 0.5 p.u. and 1.0 p.u., respectively; U_{dl} and U_{dh} are 0.5 p.u. and 0.9 p.u., respectively. The maximum recovery period of single CF is 160 ms. The DC emergency power control reference $\Delta P_{\mathrm{DC\_max}}$ is limited to 1.2 times of the rated active power to avoid the considerable effect of the DC emergency power control on the voltage magnitude at the AC grid. That is, the maximum emergency power control amount of the DC converter is 12.0 p.u.

A three-phase short circuit occurs at bus B3 at 15 s and is cleared 0.4 s later. The RMS voltage of bus B3 is reduced to 0.94 p.u., and the short-circuit fault causes continuous CFs at the DC_1 inverter station. Figure 6 presents the simulated output power and extinction angle of the DC_1 inverter station. As shown in the figure, three continuous CFs at the DC_1 inverter are caused by the short-circuit fault and lead to the continuous DC-transmitted power sag. The maximum recovery power during continuous CF P_{dc1} = 9.7 p.u. can be calculated using (4). The red dotted line in Figure 6a represents the output power of the inverter calculated using (5), which is basically consistent with the simulated power waveform.

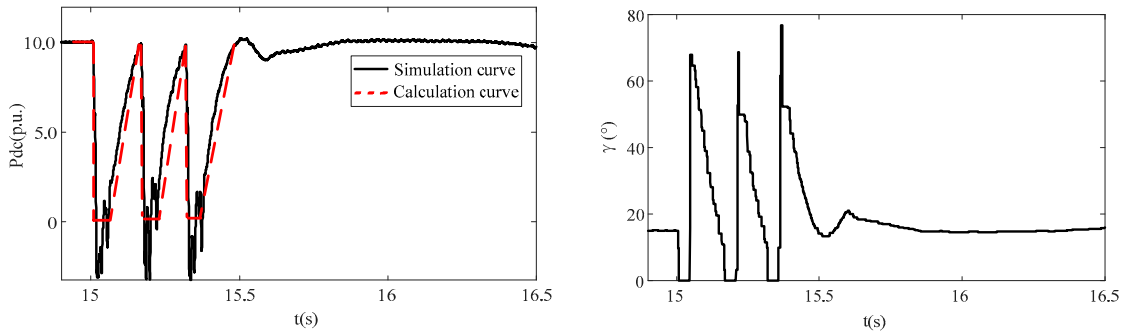

(**a**) Output power (**b**) Extinction angle

Figure 6. Operation characteristic of DC_1 under continuous CFs.

Figure 7 shows the transmitted power and extinction angle of the DC_2 inverter station. Under the influence of the continuous CFs of DC_1, the delivered active power and extinction angle of the DC_2 inverter output fluctuate slightly, and power fluctuation is approximately 5% of the rated transmitted power. The extinction angle does not decrease considerably, and no CF occurs at the DC_2 inverter.

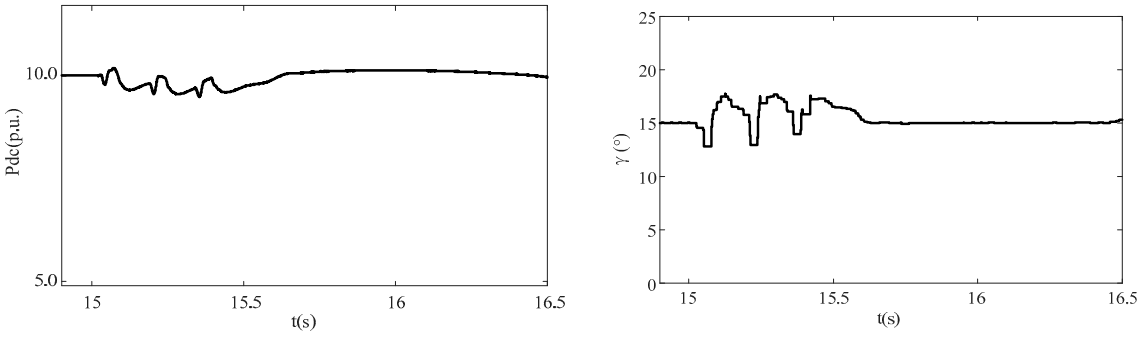

(**a**) Output power (**b**) Extinction angle

Figure 7. Operation characteristic of DC_2 under continuous CFs.

The variation in rotor angle difference between G1 and G2 is depicted in Figure 8. The continuous DC power sag causes the first swing angle instability in the sending-end system. Given that three

occurrences of continuous CFs will result in the instability of the sending-end system, DC should be blocked before the third CF occurrence and a corresponding generator tripping strategy should be adopted to ensure the stability of the sending-end system.

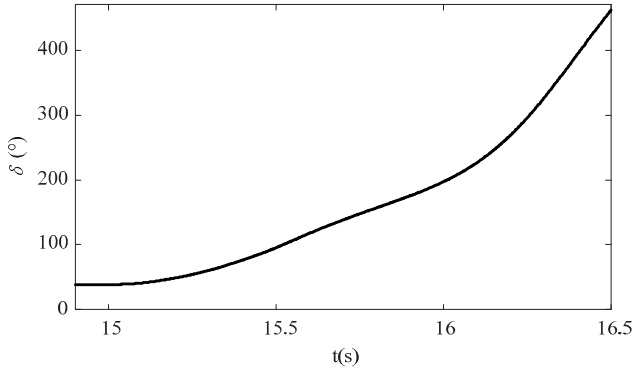

Figure 8. Rotor angle difference between G1 and G2.

5.1. Simulation Comparison under Different Control Methods

Different emergency power control methods are adopted for comparison to verify the effectiveness of the proposed control method. The DC power energy compensation modulation method adopted in [12] is selected as the conventional control method (Case 1). The emergency control reference is calculated and implemented at the end of the continuous CFs. The power control reference of DC_2 is 12.0 p.u. based on the control method, and the auxiliary generator tripping of 4.0 p.u. should be implemented in Area 1. In accordance with the emergency power control method (Case 2) proposed in Section 4, the exit time of the DC emergency power control is set as 1.5 s after the fault. Figure 9 shows the variation in delivered power of the DC_2 inverter and the equivalent rotor angle under different control methods.

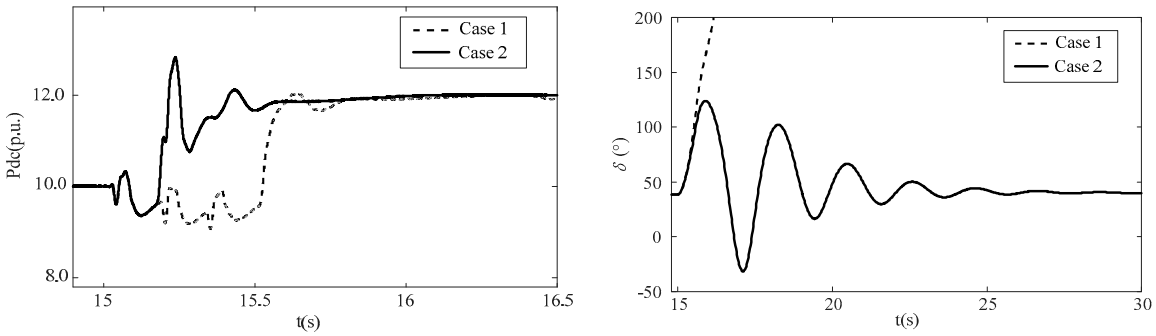

(**a**) Delivered power by inverter of DC_2 (**b**) Rotor angle difference between G1 and G2

Figure 9. Control effect under different control method.

The simulation results presented in Figure 9 indicate that if the emergency power control is implemented after the continuous CFs, then the rotor angle of the sending-end grid will lose stability. The acceleration and deceleration areas are calculated in real time on the basis of the proposed calculation method of the emergency control reference. The emergency power control is started once the second CF is detected, and the DC power control reference is adjusted to 12.0 p.u. to ensure the stability of the first swing of the sending-end system. Once the commutation process returns to normal, the system can immediately recover to normal operation. Compared with the conventional control method, the proposed emergency power control can be enabled in advance, and thus, the system stability margin can avoid insufficiency due to an excessive power angle change

at the end of continuous CFs. Figure 10 shows the transmission power and extinction angle of DC_1 under the proposed emergency power control. It can be seen that the proposed emergency control does not affect the operating characteristics of DC_1.

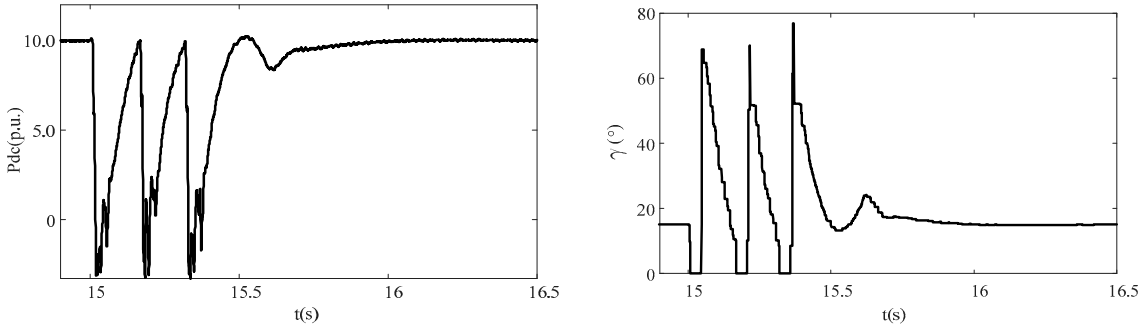

(**a**) Output power (**b**) Extinction angle

Figure 10. Operation characteristic of DC_1 under continuous CFs.

5.2. Simulation Comparison under Different Capacity Ratios

In order to verify the adaptability of the proposed control method under different DC capacity ratios, the transmitted capacity of DC_1 is adjusted to 6.0 p.u. and generator capacity in Area 1 should be correspondingly reduced 4.0 p.u. Similarly, a three-phase short circuit occurs at bus B3 at 15 s and is cleared 0.4 s later. Three continuous CFs of DC_1 are produced by this short-circuit fault. Figure 11 shows the variation in output power of the DC_2 inverter and the equivalent rotor angle under different control methods with varying DC capacity ratios. Figure 12 shows the transmission power and extinction angle of DC_1 under the proposed emergency power control. As shown in Figure 11, the continuous sag of DC power causes the instability of first swing in the sending-end system. The instability of the sending-end gird can be avoided using both control methods. In particular, the conventional control method improves the DC_2 control reference to 12.0 p.u. and the 2.0 p.u. generator will be tripped in Area 1. Using the proposed control method, the emergency power control of DC_2 can be enabled at the initiation time of the third CF, and the emergency power control reference of DC_2 is approximately 12.0 p.u., which ensures the stability of the sending-end grid. Compared with the conventional control method, the proposed control method can reduce generator tripping capacity at the sending-end grid. The simulation results show that the threshold time and control reference of the proposed emergency power control depend not only on the times of CFs, but also on the transmission capacity of DC system where continuous CFs occur.

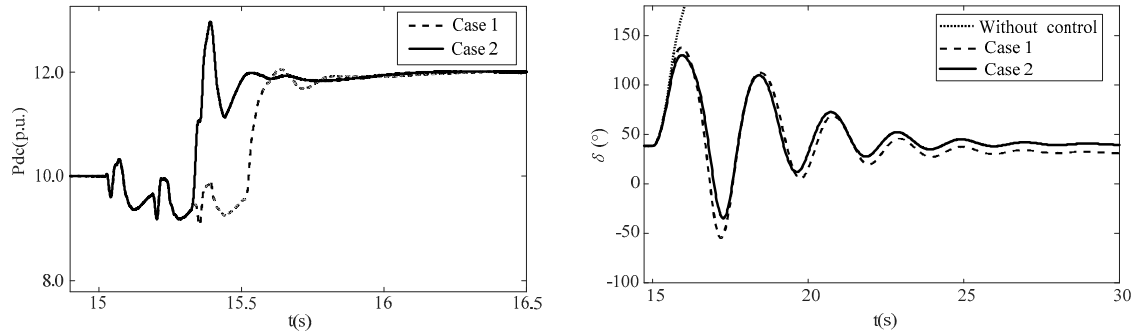

(**a**) Delivered power by inverter of DC_2 (**b**) Rotor angle difference between G1 and G2

Figure 11. Control effect under different control method.

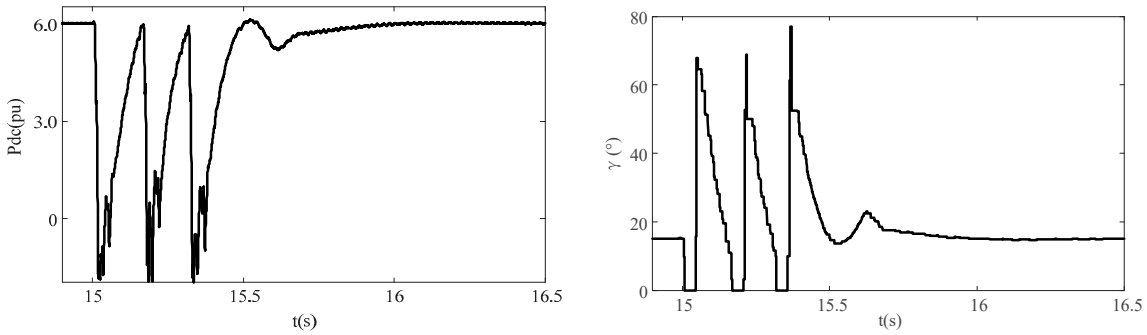

(**a**) Output power (**b**) Extinction angle

Figure 12. Operation characteristic of DC_1 under continuous CFs.

5.3. Influence of Reactive Power Variation on the Control Effect

Large sag of the active power transmitted by the DC system during continuous CFs is the key factor that cause the transient angle instability of the sending-end grid. However, a large variation in transmission power will also affect the reactive power characteristics at AC side of rectifier station. The influence of reactive power during CF on the sending-end AC system is mainly reflected in the transient overvoltage resulted by reactive power surplus of rectifier station [22]. The transient overvoltage at the rectifier side will increase the equivalent electromagnetic power peak of the sending-end gird to a certain extent, which causes the decrease of acceleration area and the increase of deceleration area during continuous CFs. Thus, by ignoring the influence of reactive power surplus in the proposed emergency control reference calculation method, the stability margin at the sending-end grid can be increased.

In order to verify the influence of reactive power surplus during continuous CFs on the proposed control, on the basis of the proposed control method, the reactive power compensation of 80 Mvar is inputted and removed during continuous CFs, respectively. Different power angle variation at sending-end grid can be obtained as shown in Figure 13. It can be seen that the minimum peak value of rotor angle during the first swing is achieved under the case of inputted reactive power compensation. Considering that the simulation results in Figures 9 and 11, actually, are obtained under the influence of reactive power variation. Therefore, ignoring the influence of reactive power during continuous CFs in the calculation method can increase the stability margin of the sending-end grid, which will improve the control effect of proposed control method.

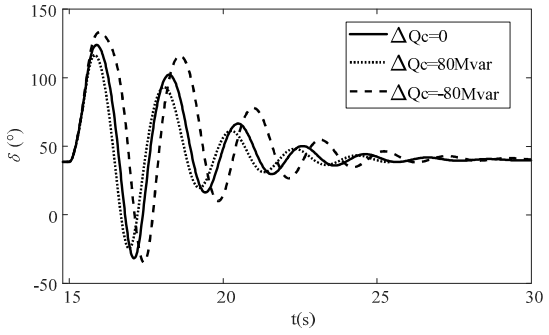

Figure 13. Comparison of control effects under reactive power variation at rectifier side.

6. Conclusions

In large-scale HVDC asynchronous interconnected power systems, continuous CFs will result in the continuous and rapid sag of DC transmission power and threaten the stability of grid. This paper presented a ride-through control method to improve the endurance capability of AC systems against

continuous CFs To quantify the influence of continuous CFs on the stability of the sending-end grid, an active output model of a DC inverter station during continuous CFs is established. In order to improve the ride through capacity during the continuous commutation failures, a rolling calculation model of the rotor angle and acceleration area of the sending-end grid during continuous CFs is established in accordance with MPC theory. On this basis, a calculation method for the emergency power control reference value is obtained. Simulation results have demonstrated this control method can improve the endurance capability of AC systems against continuous CFs, reduce the blocking risk of the DC converter during continuous CFs, and ride through continuous CFs.

Author Contributions: C.X., X.X., J.O. proposed the core idea and developed the models; C.X. and W.W. performed the simulations and analyzed the data; W.H. and J.O. revised the paper; C.X. contributed to the writing of this manuscript.

Funding: This work has been supported by the National Key R&D Program of China(2016YFB0900600), Technology Projects of State Grid Corporation of China(52170218000M).

Conflicts of Interest: The authors declare no conflict of interest.

Nomenclature

U_d	DC voltage at inverter side
I_d	DC current
N_c	Number of six-pulse thyristor bridge converter at inverter side
U_B	RMS voltage of AC system on the inverter side
γ	Extinction angle of inverter
X_c	Commutating reactance.
I_{dl}, I_{dh}	The minimum and maximum DC current reference value
U_{dl}, U_{dh}	DC voltage thresholds value
U_{rated}	Rated DC voltage
P_d	Transmitted active power of DC inverter
P_{d0}	Transmitted active power of DC inverter under steady state conditions
P_{d1}	Maximum transmitted active power during grid fault
U'_B	RMS voltage at the AC side of inverter station at the initial time of grid fault
ΔT	Duration of transmitted power sag caused by CF
t_1	Time of first CF occurs
j	Frequency of continuous CFs
P_{DC}	Sum of the active power transmitted by all DC links
x_1, x_2	Equivalent reactance of generators G1 and G2
x_{12}	Tie line reactance between bus B1 and bus B2
$E_{s1} \angle \delta_{s1}$, $E_{s2} \angle \delta_{s2}$	Internal potential and rotor angle of equivalent generators G1 and G2
U_1, U_2	Voltage amplitude at bus B1 and B2
θ_1, θ_2	Phase angle at bus B1 and B2
P_{G1}, P_{G2}	Output mechanical power of the equivalent generators
P_{L1}, P_{L2}	Load power represented by L1 and L2
P_m	Equivalent mechanical power
$P_{e\max}$	Peak value of equivalent electromagnetic power
P_{em_j}	Emergency power control reference during j-th CF
$\Delta P_{\mathrm{DC\_max}}$	Maximum emergency power support capacity of DC system
ΔP_{comp}	Minimum generator tripping capacity
P_{12}	Transmitted power from bus B_1 to bus B_2
P_{DC1}, P_{DC2}	Transmitted power by DC_1 and DC_2 inverter station
A_a, A_d	Acceleration area and deceleration area
T_{J1}, T_{J2}	Inertia time constants of equivalent generator
ω_0	Rated angular velocity
P_{DC}	Sum of the active power transmitted by all DC links
δ	Rotor angle deviations between G1 and G2
Δt	Step of piecewise linearization

References

1. Sigrist, L.; Echavarren, F.; Rouco, L.; Panciatici, P. A fundamental study on the impact of HVDC lines on transient stability of power systems. In Proceedings of the IEEE Eindhoven PowerTech, Eindhoven, The Netherlands, 29 June–2 July 2015; pp. 1–6.
2. Shah, R.; Sánchez, J.; Preece, R.; Barnes, M. Stability and control of mixed AC–DC systems with VSC-HVDC: a review. *IET Gener. Transm. Distrib.* **2018**, *12*, 2207–2219. [CrossRef]
3. Tu, J.; Pan, J.; Zhang, J.; Jia, J.; Qin, X.; Yi, J. Study on the stability mechanism of the sending-side three-machine-group system after multiple HVDC commutation failure. *IET J. Eng.* **2017**, *2017*, 1140–1145. [CrossRef]
4. Liu, C.; Zhao, Y.; Li, G.; Annakkage, U.D. Design of LCC HVDC wide-area emergency power support control based on adaptive dynamic surface control. *IET Gener. Transm. Distrib.* **2017**, *11*, 3236–3245. [CrossRef]
5. Rahimi, E.; Gloe, A.M.; Davies, J.B.; Fernando, I.T.; Kent, K.L. Commutation Failure Analysis in Multi-Infeed HVDC Systems. *IEEE Trans. Power Deliv.* **2011**, *26*, 378–384. [CrossRef]
6. Tu, J.; Zhang, J.; Bu, G.; Yi, J.; Yin, Y.; Jia, J. Analysis of the sending-side system instability caused by multiple HVDC commutation failure. *CSEE J. Power Energy Syst.* **2015**, *1*, 37–44. [CrossRef]
7. Jia, J.; Zhang, J.; Zhong, W.; Tu, J.; Yu, Q.; Yi, J. Research on the security and stability control measures of the sending side system coping with multiple parallel-operation HVDCs simultaneous commutation failure. *Proc. CSEE.* **2017**, *37*, 6320–6327.
8. Liu, H.; Liu, B.; Chen, Z. Impact and suppression measures of repeated and simultaneous commutation failure in multiple HVDC power transmission system between two regional power grids. *High Volt. Eng.* **2016**, *42*, 3315–3320.
9. Zhuang, W.; Li, D.; Yu, Z.; Li, H.; Liu, T.; Li, Z. Security and Stability Control System Coping With Simultaneous Multi-UHVDC Commutation Failure. *Power Syst. Technol.* **2016**, *40*, 3420–3426.
10. Kundur, P. *Power System Stability and Control*, 1st ed.; McGraw Hill: New York, NY, USA, 1994; pp. 533–543.
11. Kwon, D.; Kim, Y.J.; Moon, S.I. Modeling and analysis of an LCC HVDC system using DC voltage control to improve transient response and short-term power transfer capability. *IEEE Trans. Power Del.* **2018**, *33*, 1922–1933. [CrossRef]
12. Wang, S.; Tang, F.; Liu, D.; Zhou, S.; Liu, F.; Hou, Y. DC Power Energy Compensation Modulation Method Coping With Simultaneous Multiple HVDC Commutation Failures. *Power Syst. Technol.* **2018**, *42*, 2876–2884.
13. Zhou, Y.; Wu, H.; Song, Y.; Ling, W.; Lou, B.; Deng, H. Analyses of static and dynamic reactive power allocation between synchronous compensators and shunt capacitors to counter commutation failures. *Int. Trans. Electr. Energ. Syst.* **2018**, *28*, 1–14. [CrossRef]
14. Guo, C.; Liu, Y.; Zhao, C.; Wei, X.; Xu, W. Power Component Fault Detection Method and Improved Current Order Limiter Control for Commutation Failure Mitigation in HVDC. *IEEE Trans. Power Del.* **2015**, *30*, 1585–1593. [CrossRef]
15. Mirsaeidi, S.; Dong, X.; Tzelepis, D.; Said, D.M.; Dysko, A.; Booth, C. A Predictive Control Strategy for Mitigation of Commutation Failure in LCC-Based HVDC Systems. *IEEE Trans. Power Electron.* **2019**, *34*, 160–172. [CrossRef]
16. Li, M. Characteristic Analysis and Operational Control of Large-Scale Hybrid UHV AC/DC Power Grids. *Power Syst. Technol.* **2016**, *40*, 985–991.
17. He, J.; Tang, Y.; Zhang, J.; Guo, Q.; Yi, J.; Bu, G. Fast calculation of power oscillation peak value on ac tie-line after HVDC commutation failure. *IEEE Trans. Power Syst.* **2015**, *30*, 2194–2195. [CrossRef]
18. Darabian, M.; Jalilvand, A. Improving power system stability in the presence of wind farms using STATCOM and predictive control strategy. *IET Renew. Power Gener.* **2018**, *12*, 98–111. [CrossRef]
19. Zhou, X.; Sun, H.; Zhao, B.; Wen, J.; Waqar, A. Applying high-voltage direct current emergency control to suppress the peak value of ultra-high-voltage tie-line power oscillation. *IET Gener. Transmiss Distrib.* **2015**, *9*, 2485–2492. [CrossRef]
20. Elizondo, M.A.; Fan, R.; Kirkham, H.; Ghosal, M.; Bernal, F.W.; Schoenwald, D.; Lian, J. Interarea Oscillation Damping Control Using High Voltage DC Transmission: A Survey. *IEEE Trans. Power Syst.* **2018**, *33*, 6915–6923. [CrossRef]

21. Du, Z.; Gan, D.; Liu, Y.; Xia, D. A fast numerical integration method for power system on line dynamic security assessment. *Proc. CSEE.* **1996**, *16*, 29–32.
22. Tu, J.; Pan, Y.; Zhang, J.; Zeng, B.; Jia, J.; Yi, J. Transient reactive power characteristics of HVDC during commutation failure and impact of HVDC control parameters. *IET J. Eng.* **2017**, *2017*, 1134–1139. [CrossRef]

© 2019 by the authors. Licensee MDPI, Basel, Switzerland. This article is an open access article distributed under the terms and conditions of the Creative Commons Attribution (CC BY) license (http://creativecommons.org/licenses/by/4.0/).